University of Tehran Press

Magnetotelluric Evidence for Electrical Anisotropy in the Sabalan Geothermal Reservoir, Northwestern Iran

Mirhadi, Z. S.[1] | Habibian Dehkordi, B.[2] ✉

1. Department of Earth Physics, Institute of Geophysics, University of Tehran, Tehran, Iran. E-mail: zahramirhadi@ut.ac.ir
2. **Corresponding Author**, Department of Earth Physics, Institute of Geophysics, University of Tehran, Tehran, Iran. E-mail: bhabibian@ut.ac.ir

Abstract
Ignoring electrical anisotropy, if present, results in inaccurate modeling of electromagnetic data and unreliable subsequent interpretation. Its identification through the data analysis procedure, therefore, can lead to the selection of the correct algorithm for modeling and inversion and ultimately trustworthy interpretation. In this study, a part of the magnetotelluric data acquired on Sabalan volcano, located in northwestern Iran, was examined in terms of the presence of electrical anisotropy. For this purpose, penetration depths, anisotropy coefficients, phase tensor, induction vectors, and distortion parameters were considered. The results confirm significant signatures for anisotropic features in the area in the form of different depths of two polarizations, high anisotropy magnitudes, and consistent deviation of the phase tensor main axes and anisotropy directions from the regional trend. This is consistent with the outflow direction towards the Moil valley, indicated by previous studies and the high density of fractures and faults related to the setting of hydrothermal reservoirs as the main path of fluid flow.

Keywords: Magnetotellurics, Electrical Anisotropy, Electrical Conductivity, Sabalan Mountains, Phase Tensor.

1. Introduction
There are many examples of the use of electromagnetic methods alone or in combination with other methods (Hosseini et al., 2021) in the successful characterization of geothermal reservoirs, which have increased over the last years. Although other EM methods such as transient electromagnetic (TEM) and DC resistivity are also used, the magnetotelluric (MT) method due to its larger penetration depth and greater capability has been more extensively applied for the exploration of geothermal reservoirs. Comprehensive reviews are given by Spichack & Manzella (2009) and Mũnoz (2014).

Anisotropy as a factor that is closely related to the tectonic state and evolution of geological structures is of great importance in interpretation. Due to the difficulty of its identification in the magnetotelluric transfer functions (Christensen, 2000), and the complexity of its inclusion in the modeling procedure, however, the existence of anisotropy is ignored in many cases.

Anisotropy, on the other hand, is not always detectable; especially when it has a similar orientation to the target structures, that occurs within 3D environments, or is masked by galvanic distortion effects (Martí, 2014). In addition, an isotropic conductivity distribution, if not well resolved, can produce an effect similar to an anisotropic structure. The isotropic approximation of anisotropic environments may create false structures through inversion and lead to inaccurate interpretation. A review of the topic can be found in Martí (2014).

Although the Earth is anisotropic on all scales (Jones, 2012), anisotropy estimation depends on the scale of measurement. This means that conductivity may be isotropic on a microscopic scale - there is no inherent anisotropy in the grains - but anisotropy appears on larger scales (Miensopust & Jones, 2011). Most rocks are anisotropic according to the drilling logs. Examples are rocks under pressure or faults that in many cases have higher conductivity than the

background. Crash zones in crystalline environments, for example, are common phenomena, that if they have preferential orientation over the scale of measurement, can produce azimuthal anisotropy (Li & Pedersen, 1991).

Sabalan geothermal area is a high temperature, about 270 degrees Celsius at a depth of 2 km, water-dominated system, located in the northwest of Iran. Electrical resistivity is related to temperature, the presence of hydrothermal fluids, and clay minerals. An ideal hydrothermal system consists of a heat source, groundwater fluids to transfer or store heat (reservoir), and an impermeable confined structure on the top.

Iran renewable energy organization (SUNA) has conducted electromagnetic measurements in three different time schedules related to 1998, 2007 and 2009 in this area. In 1998, measurements, including magnetotellurics, were carried out in the Sabalan region and several major conductivity anomalies were identified the largest of which was in the Moil Valley in the west of the region. Since the selected period interval for these measurements did not achieve the predicted penetration depth, in 2007, additional measurements were conducted on 28 new stations to determine the reservoir center and drilling targets. Insufficient coverage of the stations, however, especially in the eastern and southeastern parts led to new data collection. Thus, in 2009, 50 new and 10 repetitive stations were measured in an area of about 150 km^2 and their locations can be seen in Figure 1.

In this study, part of the magnetotelluric data collected in the Sabalan geothermal area, MT data from the years 2007 and 2009 (Figure 1), have been examined aiming at investigating the presence of electrical anisotropy. To identify the possible anisotropy, Niblett-Bostick penetration depths are obtained; impedance and phase tensors are used; anisotropy coefficients are calculated and distortion level is evaluated.
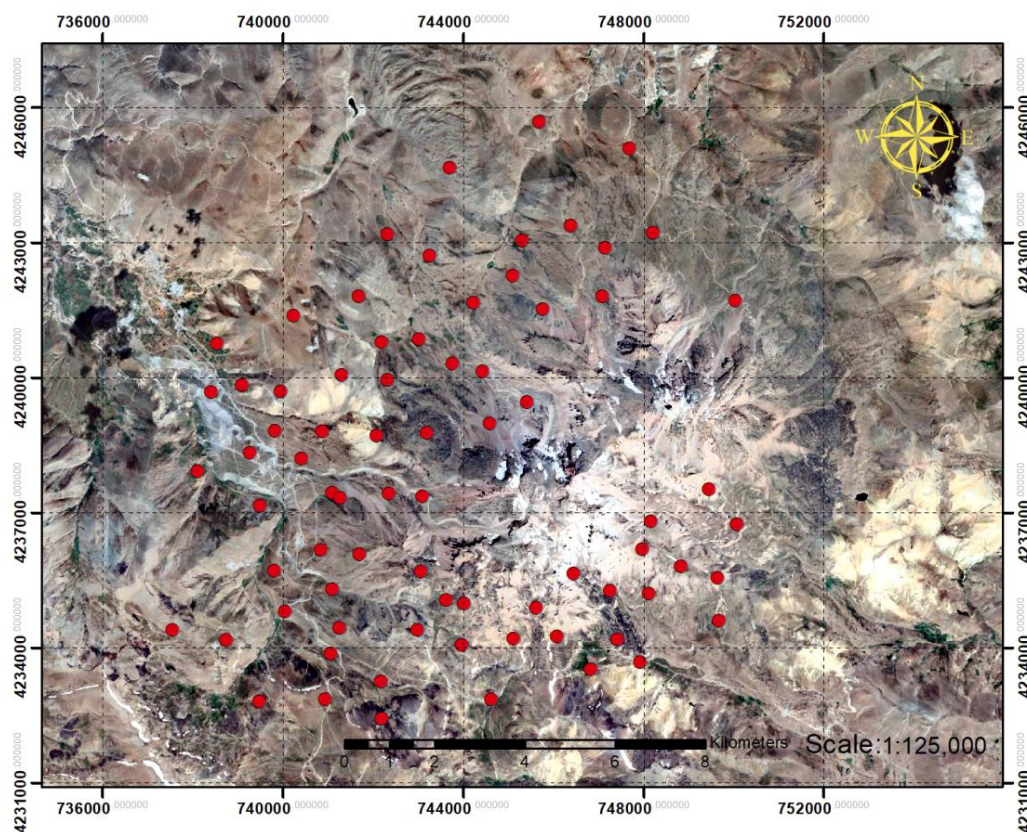
Stations Map

Figure 1. Location of magnetotelluric stations on Sabalan volcano.

2. Geological Setting

Sabalan is a stratovolcano, extending in an east-west direction, located in Ardabil province, northwest of Iran. Periods of volcanic activity provide the heat source for a high-enthalpy geothermal reservoir, which is accompanied by numerous surface manifestations such as well-known hot springs in the region, most of which are in the Moil Valley.

Consecutive subductions and continental collisions, beginning in the early Mesozoic and continuing to the present time have imposed a very complex compressional setting in northwestern Iran, where the Sabalan Mountains are located.

Altered Pliocene volcanic, an unaltered Pleistocene trachydacite dome and Quaternary terrace deposits are the main surface exposures of the study area, Moil valley. They are consequences of volcanic activity and subsequent alteration and are divided into the following units in order of increasing age (Bogie et al., 2000; Bromley et al., 2000; KML, 1998; Yousefi et al., 2009):

- Quaternary alluvium, fan and terrace deposits
- Pleistocene post-caldera trachy andesitic lava flows, domes and lahars
- Pleistocene syn-caldera trachydacitic to trachyandesitic domes, lava flows and lahars
- Pliocene pre-caldera trachyandesitic lavas, tuffs and pyroclastics.

3. Magnetotelluric Responses

In the magnetotelluric method, the underground distribution of electrical resistivity is obtained by simultaneously measuring the natural fluctuations of electric and magnetic fields on the earth's surface. The horizontal components of the electric and magnetic field are related by the impedance tensor (Z), and the tipper vector (T) relates the vertical magnetic field to its horizontal components (e.g., Schmucker, 1970; Vozoff, 1972):

$$E = ZH \qquad (1)$$

$$H_z = TH , \qquad (2)$$

where E and H indicate electric and magnetic fields, respectively. Apparent resistivity (ρ) and phase (φ) are usually calculated from impedance components as more intuitive quantities:

$$\rho_{ij} = \frac{1}{\mu_0 \omega} |Z_{ij}|^2 , \qquad \varphi_{ij} = tan^{-1}(\frac{ImZ_{ij}}{ReZ_{ij}}) \qquad (3)$$

The phase information contained in the impedance tensor can be represented by a 2×2 phase tensor (Φ) obtained from the ratio of the imaginary (Y) and real parts (X) of the impedance tensor (Caldwell et al., 2004):

$$\Phi = \frac{Y}{X} \qquad (4)$$

$$\begin{bmatrix} \Phi_{11} & \Phi_{12} \\ \Phi_{21} & \Phi_{22} \end{bmatrix} = $$
$$\frac{1}{det(X)} \begin{bmatrix} X_{22}Y_{11} - X_{12}Y_{21} & X_{22}Y_{12} - X_{12}Y_{22} \\ X_{11}Y_{21} - X_{21}Y_{11} & X_{11}Y_{22} - X_{21}Y_{12} \end{bmatrix} \qquad (5)$$

Generally, the phase tensor is not symmetric and its components do not coincide with the corresponding components of the impedance tensor. The important property of the phase tensor as a tool for dimensionality analysis and strike estimation is that it is not affected by galvanic distortions.

4. Electrical Anisotropy in the Sabalan Geothermal Field

In an anisotropic Earth, electrical conductivity (σ) is a direction-dependent quantity and therefore has a tensorial nature:

$$\begin{pmatrix} J_x \\ J_y \\ J_z \end{pmatrix} = \begin{pmatrix} \sigma_{xx} & \sigma_{xy} & \sigma_{xz} \\ \sigma_{yx} & \sigma_{yy} & \sigma_{yz} \\ \sigma_{zx} & \sigma_{zy} & \sigma_{zz} \end{pmatrix} \begin{pmatrix} E_x \\ E_y \\ E_z \end{pmatrix} \qquad (6)$$

where J is the current density. In intrinsic anisotropy, the directional dependence of the conductivity occurs at all scales, while in the case of macroscopic or structural anisotropy, the Earth is composed of isotropic components constructing anisotropic bulk conductivity.

Based on Euler's rotations, the conductivity tensor can be diagonalized and expressed with six parameters: three conductivities $(\sigma_x, \sigma_y, \sigma_z)$ in the principal directions and three corresponding angles:

$$\sigma'(x,y,z) = R.\sigma.R^T = \begin{bmatrix} \sigma_x & 0 & 0 \\ 0 & \sigma_y & 0 \\ 0 & 0 & \sigma_z \end{bmatrix} \qquad (7)$$

R is a rotation matrix obtained from three initial rotations with strike (α_S), deep (α_D), and slant (α_L) angles (Martí, 2014; Pek & Santos, 2002; Pek & Verner, 1997). If all three angles are zero, the conductivity tensor

is diagonal in the measurement coordinates.
While differences in penetration depths between TE- (electric field parallel to the strike direction) and TM- (magnetic field parallel to the strike direction) modes occur due to the different attenuation of EM wave propagation (Jones, 2006), the difference can be more significant in the case of anisotropy. The presence of different values of resistivity in different directions due to anisotropy causes the x-y and y-x polarizations to represent MT responses of structures at different depths (Jones, 2006). Since the skin depth formula is an exact relationship only for a homogenous half-space, Niblett-Bostick transformation is used to transform period to depth. Transformed data, that is Niblett-Bostick penetration depth (h_{NB}) and resistivity at this depth $(\rho_{NB}(h_{NB}))$ are given by Jones (1983):

$$h_{NB} = \sqrt{\frac{\rho_a(T)T}{2\pi\mu_0}} \quad , \quad \rho_{NB}(h_{NB}) = \rho_a(T)(\frac{\pi}{2\varphi(T)} - 1) \quad (8)$$

where $\rho_a(T)$ and $\varphi(T)$ are apparent resistivity and phase at period T, μ_0 is the free space permeability.

To examine the data from this point of view, Niblett-Bostick depths are computed for two polarizations and are shown in the diagram in Figure 2. The difference between the Niblett-Bostick depths of the two modes is about 50 km for the same periods and could be indicative of changes in resistivity with direction.

In the next step, the anisotropy coefficients are calculated as more reliable criteria for the presence of electrical anisotropy, and their distribution is shown in the map in Figure 3. This is done by rotating data at 1° intervals in the 180° range and obtaining the Niblett-Bostick transformed data (ρ_{NB}) at any angle. From this set, the largest ρ value and its related direction (Θ_{max}) are determined. Anisotropy is then obtained at a certain depth (h) from Equation (9) (Jones et al., 2014):

$$aniso = \log(\rho_{NB}(h, \Theta_{max}))\_\log(\rho_{NB}(h, \Theta_{max} + 90°)) \quad (9)$$

The arithmetic average of the two modes is used to drive the depth at each site. The anisotropy magnitude is the ratio between maximum and minimum values of conductivity and the anisotropy direction corresponds to the direction of maximum conductivity. Low values of coefficients are observed in a significant number of periods and stations. It should be noted, of course, that the estimated anisotropy is theoretically a measure of the minimal value (Jones et al., 2014). Anisotropy directions or direction of maximum resistivities are also plotted on the map in Figure 3. Stations in the western part of the map, marked with circles have consistently the highest anisotropy coefficients for periods of 37 to 217 seconds and are considered the first set of candidates to be examined further in terms of anisotropy. A point with a very high value of anisotropy appearing on all maps is ignored. Because multiple sites should be checked to study anisotropy as well as this high value occurs unacceptably at all periods.
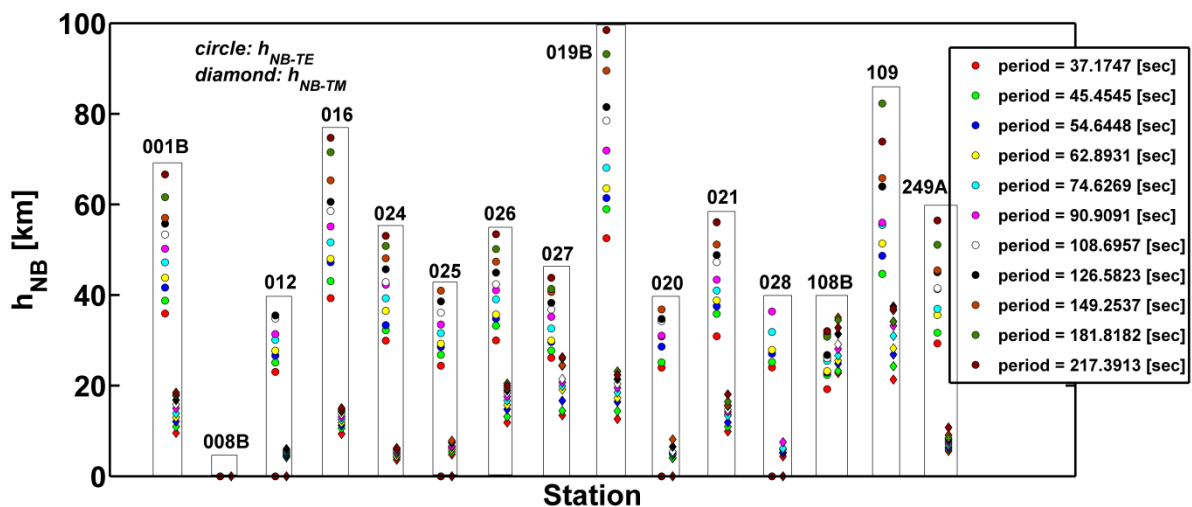

Figure 2. Niblett-Bostick penetration depths of TE (circle and left of the column) and TM (diamond and right of the column) modes.
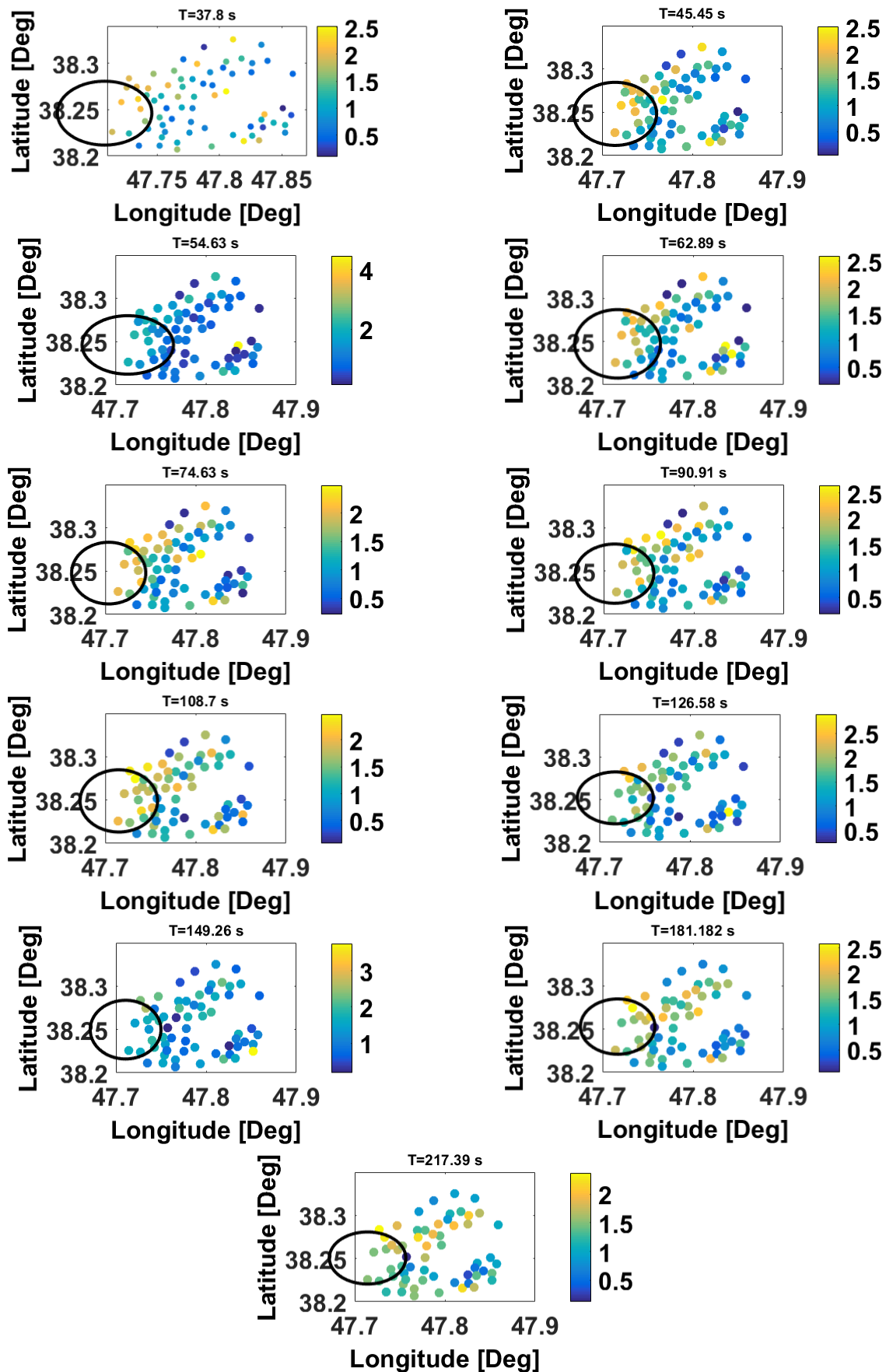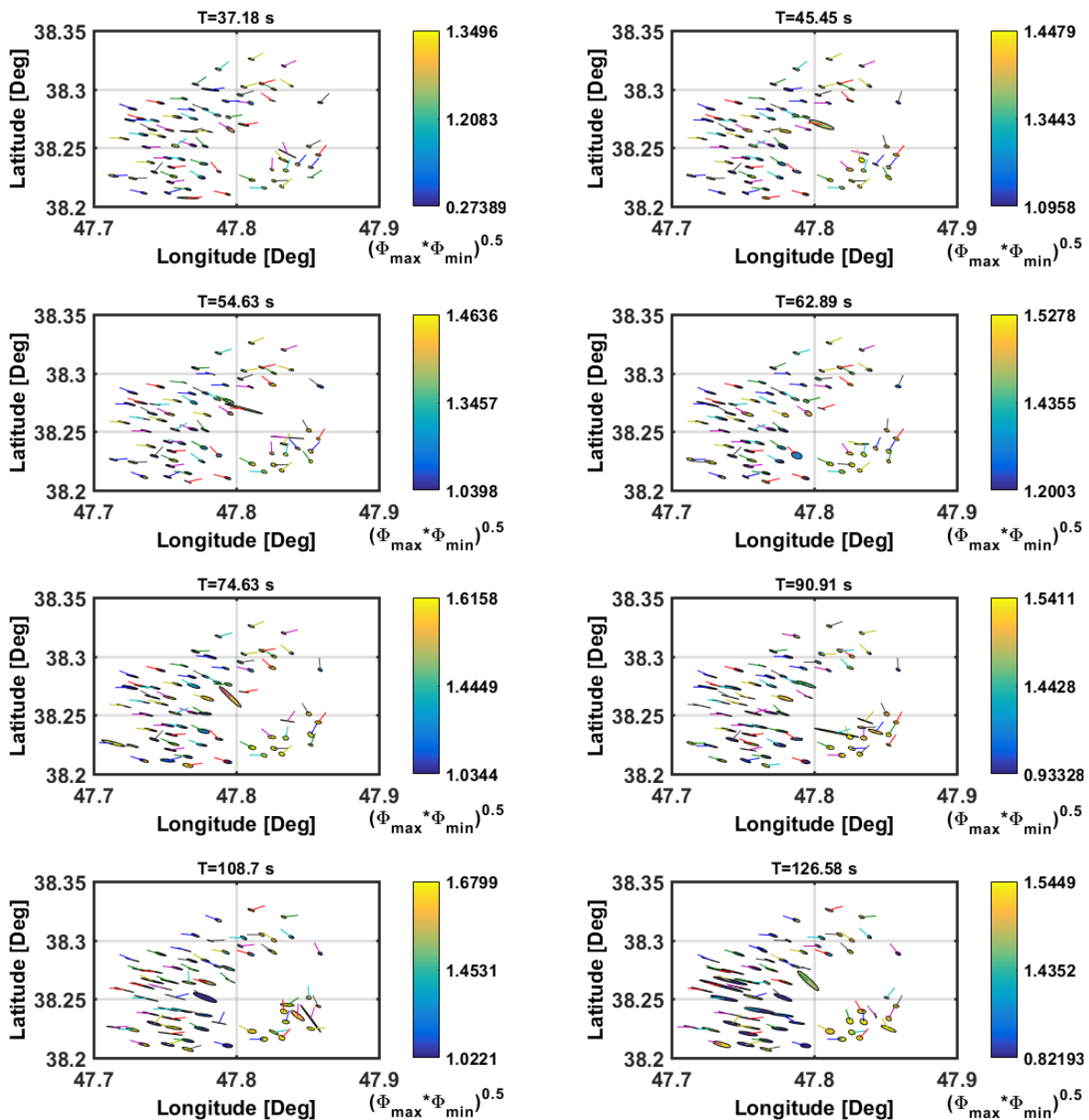
Figure 3. Map of anisotropy magnitudes for all stations.

One of the criteria commonly used to detect anisotropy is the impedance phase splitting. However, the interference of isotropic structures with galvanic distortion can also cause the combination of orthogonal polarizations and lead to the splitting of impedance phases. Therefore, using responses such as phase tensor that is not affected by distortion is particularly important for the detection of anisotropy. In Figure 4, phase tensor ellipses are displayed. Periods are selected according to anisotropy coefficients within the period interval, which is the most probable for the occurrence of anisotropy behavior. The very elongated phase tensor ellipses indicate a degree of structural anisotropy in which the flow of horizontal current is direction-dependent (Bedrosian, 2016). On the other hand, splitting of the main phases of the phase tensor is caused by vertical gradients of anisotropy and not anisotropy itself (Heise et al., 2006; Booker, 2014). Ellipses close to the circle or without phase splitting, therefore, are not sufficient conditions for the absence of anisotropy. The elongation of the phase tensor ellipses and their main axes orientation in this period range and on this part of the map are relatively uniform and consistent with the directions of anisotropy. This direction confirms about 70° to the west.
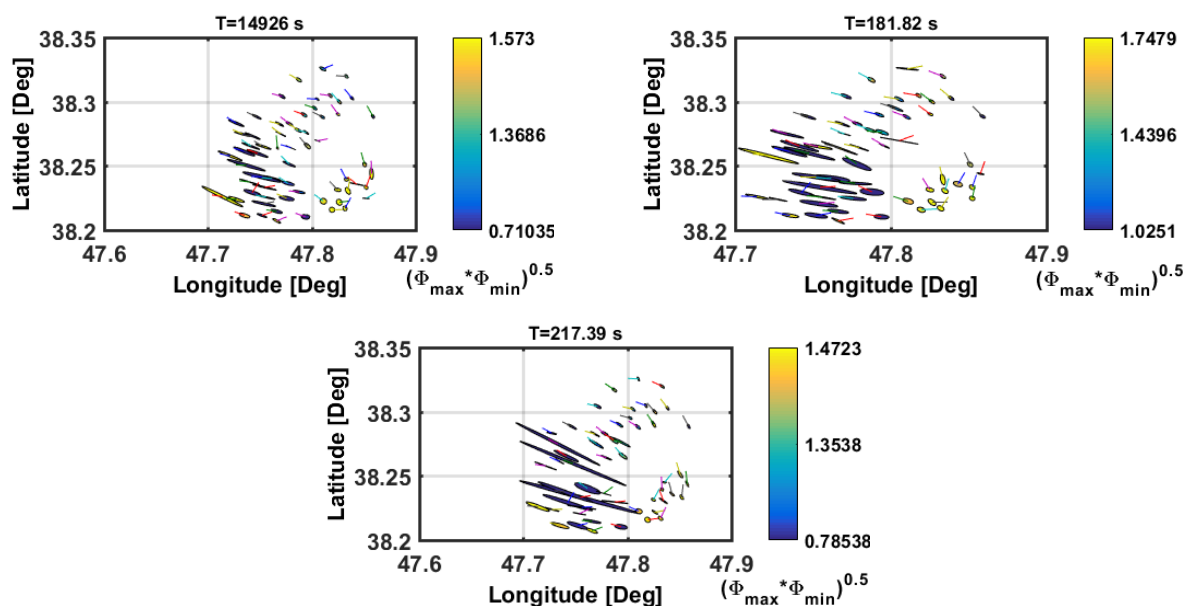
Figure 4. Map of phase tensor ellipses color coded with $\sqrt{\Phi_{max}\Phi_{min}}$.

The direction of the regional geoelectric strike, according to previous studies (Oskooi et al., 2015), is east-west, and therefore, the above behavior is considered a consistent deviation of the dominant trend of the region, although the presence of three-dimensional effects and other complexities makes this direction an approximate one.

Constant phase tensor split with the small magnitude of induction vectors is a known signature of anisotropy (Jones, 2012). On the other hand, induction vectors that are perpendicular to the strike direction in two-dimensional cases show different behavior in the presence of anisotropic structures. According to the map of induction vectors for the Sabalan region, not shown here, most of them have very small magnitudes and completely irregular orientations.

Small conductivity features affect the long-period electric field data and produce galvanic distortions. In the procedure of distortion analysis, a distortion tensor that is independent of the measurement location can be considered as a sign of possible anisotropy. Here, a set of WAL rotational invariants (Weaver et al., 2000), implemented in the WALDIM code (Martí et al., 2009) has been applied and the distribution of twist and shear angles as the determinable part of the distortion tensor (Bibby et al., 2005) is obtained. The results are presented for example sites in Table 1. In an overview, the angles do not show very high values confirming low to medium levels of distortion affecting the data. In the case of anisotropy, the same distortion matrix for different locations is expected (Bibby et al., 2005). Since galvanic distortion depends on the relationship between near-surface local heterogeneity and the background, the interpretation can be quite complex. The stations in question, however, show approximately similar values for shear and twist angles that are unlikely to be due to the same distorting heterogeneity.

5. Conclusion
In most geothermal systems, the flowing fluid in the spaces created by fractures and faults is heated by a heat source, e.g. a partially melted magma from a volcanic system as the most common source. The occurrence of electrical anisotropy, therefore, can be considered as a possible phenomenon in such environments. The preferred orientation of fluids and fractures is considered as one of the important sources of anisotropy in the crust. This makes geothermal areas the main candidates to be electrically anisotropic.

Table 1. Values of shear and twist angles for example sites.

site	period (s)	shear (°)	twist (°)	site	period (s)	shear (°)	twist (°)
027	62.9	19.86	29.78	017	90.9	22.94	21.73
221	62.9	20.94	19.24	027	90.9	23.56	35.12
010	62.9	24.32	24.66	025	90.9	23.05	52.41
025	62.9	29.17	56.41	221	90.9	27.87	28.66
026	62.9	33.75	27.42	010	90.9	27.73	30.15
109	62.9	31.65	26.89	109	90.9	28.65	31.33
015	62.9	43.63	20.38	012	90.9	25.84	54.3
016	62.9	46.11	23.89	024	90.9	33.07	49.34
020	62.9	45.46	31.9	027	109	26.07	37.17
025	74.6	24.86	54.85	015	109	28.13	50.28
010	74.6	25.51	29.96	020	109	26.58	52.86
012	74.6	29.6	57.79	024	109	30.75	48.15
020	74.6	26.02	56.55	013	109	39.07	22.38
109	74.6	31.42	29	109	109	36.76	33.07
020	90.9	17.36	55.58	221	109	35.88	31.06

In the Sabalan geothermal region, like other geothermal settings, due to the presence of faults and fractures preparing paths of fluid flow, there is a possibility that features are electrically anisotropic. A set of direct and indirect MT responses were acquired in the Sabalan geothermal region and their behavior was examined in terms of the presence of anisotropy. Large differences in penetration depths between principal polarizations (TE- and TM-mode) of the impedance tensor, high values of anisotropy ratio, and consistent deviation of the principal axes of the phase tensor ellipses are observed. Since the vertical component of conductivity cannot be determined from MT data alone, azimuthal anisotropy can only be examined here.

The examined area can be considered, accordingly, as having significant indications of anisotropy. This is justified by the existence of multiple faults in the region. It also matches well with the predicted main outflow in the Moil Valley. However, it should be kept in mind that proving the existence of anisotropy and its details requires anisotropic modeling, which is strongly suggested in the continuation of the work due to the observation of its signatures.

References
Bedrosian, P.A. (2016). Making it and braking it in the Midwest: Continental assembly and rift from modeling of Earth Scope magnetotelluric data. *Precambrian Research*, 278, 337-361.

Bibby, H.M., Caldwell, T.G., & Brown, C. (2005). Determinable and non-determinable parameters of galvanic distortion in magnetotellurics. *Geophys. J. Int*, 163, 915-930.

Bogie, I., Cartwright, A.J., Khosrawi, K., Talebi, B., & Sahabi, F. (2000). The Meshkin Shahr geothermal project, Iran. *Proceedings, World Geothermal Congress*, 997-1002.

Booker, J.R. (2014). The magnetotelluric phase tensor: A critical review. *Surv Geophys*, 35, 7-40.

Bromley, C., Khosrawi, K., & Talebi, B. (2000). Geophysical exploration of Sabalan geothermal prospects in Iran. *World Geothermal Congress*, May 28-June 10, Kyushu-Tohoko, Japan.

Caldwell, T.G., Bibby, H.M., & Brown, C. (2004). The magnetotelluric phase tensor. *Geophysical Journal International*, 158(2), 457-469.

Christensen, N.B. (2000). Difficulties in determining electrical anisotropy in subsurface investigations. *Geophysical*

Prospecting, 48, 1-19.

Heise, W., & Pous, J. (2001). Effects of anisotropy on the two-dimensional inversion procedure. *Geophys. J. Int.*, 147, 610-621.

Heise, W., Caldwell, T.G., Bibby, H.M., & Brown, C. (2006). Anisotropy and phase splits in magnetotellurics. *Physics of the Earth and Planetary Interiors*, 158(2-4), 107-121.

Hosseini, S.H., Habibian Dehkordi, B., Abedi, M., & Oskooi, B. (2021). Implications for a Geothermal Reservoir at Abgarm, Mahallat, Iran: Magnetic and Magnetotelluric Signatures. *Natural Resources Research*, *30*(1), 259-272., https://doi.org/10.1007/s11053-020-09739-8.

Jones, A.G. (1983). On the equivalence of the "Niblett" and "Bostick" transformations in the magnetotelluric method. *Journal of Geophysics*, 53(1), 72-73.

Jones, A.G. (2006). Electromagnetic interrogation of the anisotropic Earth: Looking into the Earth with polarized spectacles. *Physics of the Earth and Planetary Interiors*, 158(2-4), 281-291.

Jones, A.G. (2012). Distortion decomposition of the magnetotelluric impedance tensors from a one-dimensional anisotropic Earth. *Geophysical Journal International*, 189(1), 268-284.

Jones, A.G., Ledo, J., Ferguson, I.J., Craven, A., Unsworth, M.J., & Choteau, M. (2014). The electrical resistivity of Canada's lithosphere and correlation with other parameters: contribution from Lithoprobe and other programmes. *Can. J. Earth Sci.*, 51, 573-617.

KML. (1998). Sabalan geothermal project, Stage 1, Surface exploration, final exploration report. Kingston Morrison Limited Co. Report 2505-RPT-GE-003-for the Renewable Energy Organization of Iran (SUNA), Tehran, Iran, 83 pp.

Li, X., & Pedersen, L.B. (1991). The electromagnetic response of an azimuthally anisotropic half-space. *Geophysics*, 56(9), 1462-1473.

Martí, A., Queralt, P., & Ledo, J. (2009). WALDIM: A code for the dimensionality analysis of magnetotelluric data using the rotational invariants of the magnetotelluric tensor. *Computers & Geosciences*, 35, 2295-2303.

Martí, A. (2014). The role of electrical anisotropy in magnetotelluric responses: From modelling and dimensionality analysis to inversion and interpretation. *Surveys in Geophysics*, 35(1), 179-218.

Miensopust, M.P., & Jones, A.G. (2011). Artefacts of isotropic inversion applied to magnetotelluric data from an anisotropic Earth. *Geophysical Journal International*, 187(2), 677-689.

Mũnoz, G. (2014). Exploring for geothermal resources with electromagnetic methods. *Surv Geophysics*, 35, 101-122.

Oskooi, B., Fanaee Kheirabad, G.A., Habibian Dehkordi, B., & Nieuwenhuis, G. (2015). Three-dimensional conductivity model of the Sabalan geothermal field, NW Iran, interpreted from magnetotelluric data. *Arabian Journal of Geosciences*, 8(5), 3149-3157.

Pek, J., & Santos, F.A.M. (2002). Magnetotelluric impedances and parametric sensitivities for 1-D anisotropic layered media. *Computer and Geosciences*, 28, 939-950.

Pek, J., & Verner, T. (1997). Finite-difference modelling of magnetotelluric fields in two-dimensional anisotropic media. *Geophysical Journal International*, 128(3), 505-521.

Schmucker, U. (1970). Anomalies of geomagnetic variations in the southwestern United States, Bulletin of the Scipps Institution of Oceanography. *Marine and Petroleum Geology*, 21(5), 535-554.

Spichak, V., & Manzella, A. (2009). Electromagnetic sounding of geothermal zones. *Journal of Applied Geophysics*, 68, 459-478.

Vozoff, K. (1972). The magnetotelluric method in the exploration of sedimentary basins. *Geophysics*, 37, 98-141.

Weaver, J.T., Agarwal, A.K., & Lilley, F.E.M. (2000). Characterization of the magnetotelluric tensor in terms of its invariants. *Geophys. J. Int.*, 141, 321-336.

Yousefi, H., Noorollahi, Y., Ehara, S.,Yousefi, A., Fujimitsu, Y.N.J., & Sasaki, K. (2009). Developing the geothermal resources map of Iran. *Geothermics*, 39, 140-151.

Appendix A. Synthetic tests

Synthetic tests were performed using two anisotropic models (Figure A1) taken from Heise & Pous (2001). The first synthetic model consists of a lateral contact between an anisotropic medium with principal resistivities $\rho_{min} = 20\ \Omega.m/\rho_{amx} = 1000\ \Omega.m$ and anisotropy strike of $30°$, and isotropic model of $1000\ \Omega.m$ covered by a resistive layer of $1000\ \Omega.m$. The second synthetic model consists of a contact between $20\ \Omega.m$ and $1000\ \Omega.m$ isotropic media, underlain by an anisotropic layer of $\rho_{min} = 20\ /1000\ \Omega.m$ with anisotropy strike of $30°$. A $20\ \Omega.m$ conductive surface layer and a $5000\ \Omega.m$ resistive layer cover the model (Heise & Pous, 2001).
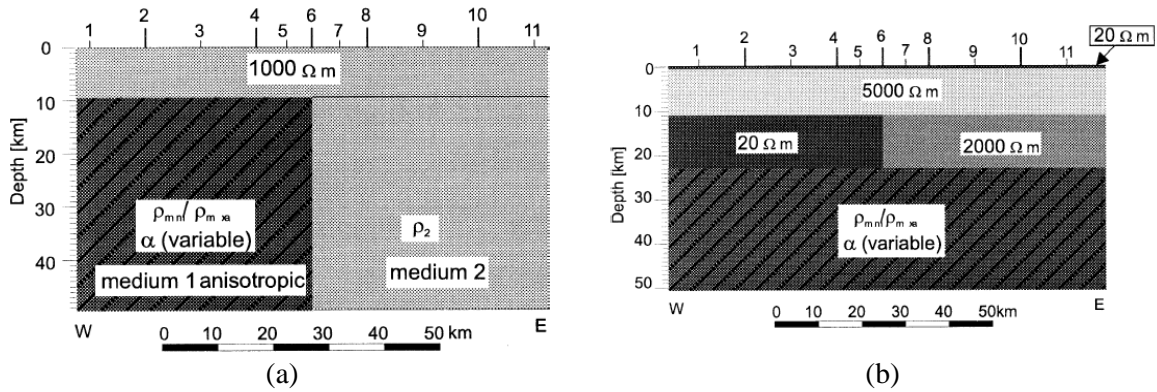

Figure A-1. The first (a) and second (b) anisotropic models used to generate synthetic data (Heise & Pous, 2001).

The synthetic data were generated using the anisotropy code of Pek & Verner (1997). Transformed data, phase tensor principal axes and anisotropy ratios were considered exactly the same way as for the real data. The results are shown in Figures A2 and A3. The elongation of the phase tensor ellipses in the corresponding parts indicates a preferred direction for the flow of electric current. This together with the high-value anisotropy ratios show the effect of anisotropic structures on the magnetotelluric responses.
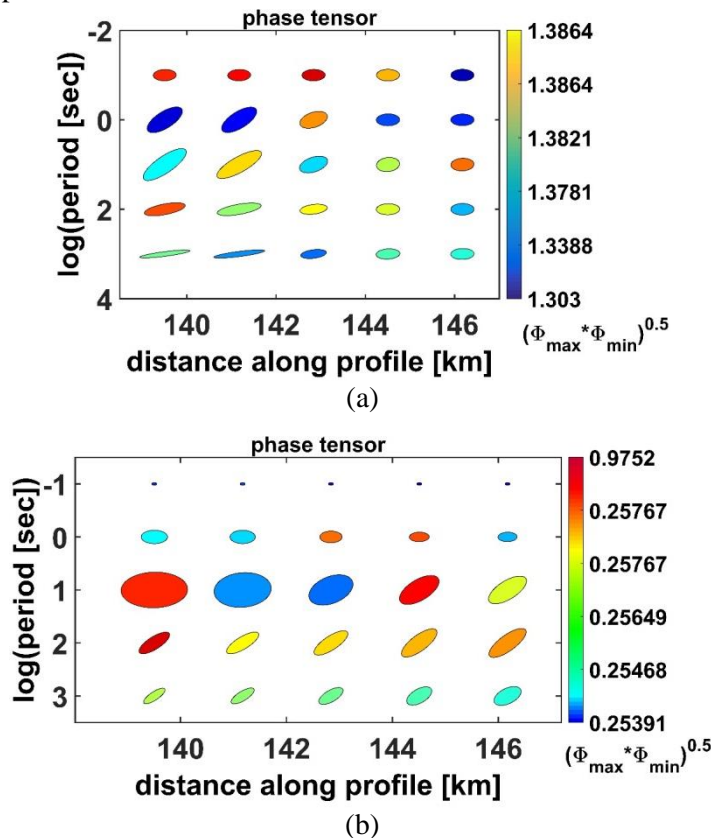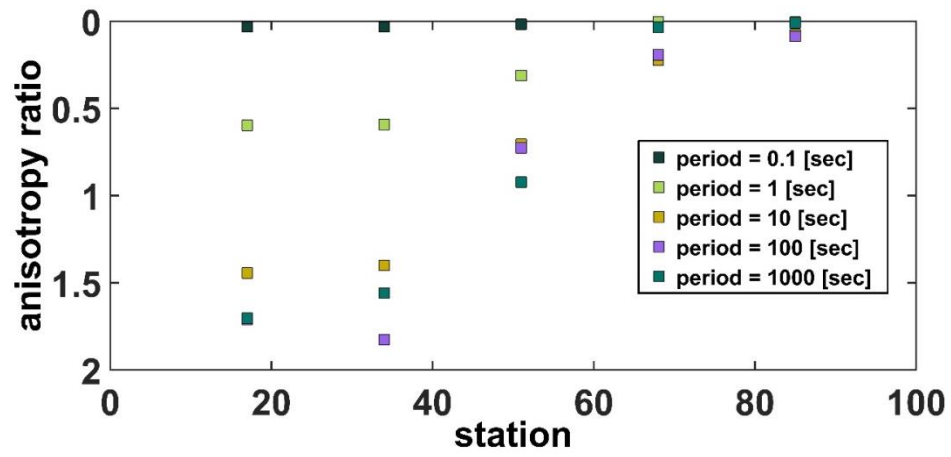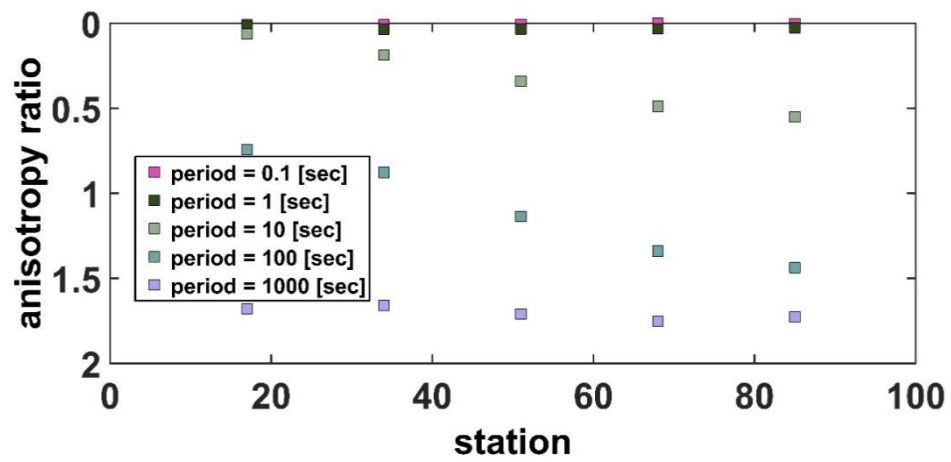

Figure A-2. Pseudo-sections of phase tensor ellipses for the first (a) and the second (b) synthetic anisotropic models.

(a)

(b)

Figure A-3. Map of anisotropy magnitudes for the first (a) and the second (b) synthetic anisotropic models.